



Magnetic Properties and Magnetocaloric Effect in $\text{Tb}_2\text{FeCrO}_6$ Double Perovskite Oxide

Silu Huang¹ · Junli Lin² · Yongyun Shu¹ · Yikun Zhang^{1,2}

Received: 12 November 2023 / Accepted: 15 February 2024
© The Minerals, Metals & Materials Society 2024

Abstract

In this work, we fabricated a polycrystalline $\text{Tb}_2\text{FeCrO}_6$ double perovskite (DP) oxide by a solid-state reaction method and determined its structural, magnetic, and magnetocaloric (MC) properties. The $\text{Tb}_2\text{FeCrO}_6$ DP oxide was found to crystallize in a DP-type structure with the $Pbnm$ space group and to undergo a paramagnetic-to-antiferromagnetic transition at a temperature of ~ 8.5 K. A large low-temperature MC effect was observed in the $\text{Tb}_2\text{FeCrO}_6$ DP oxide. The MC parameters in terms of maximum magnetic entropy changes, temperature-averaged entropy change (5 K), and relative cooling power for $\text{Tb}_2\text{FeCrO}_6$ DP oxide under a magnetic field change of 0–7 T were 12.9 J/kg K, 12.7 J/kg K, and 341.4 J/kg, respectively. These parameters were consistent with similarly high levels in recently updated MC materials, making the material a suitable candidate for low-temperature magnetic cooling applications.

Keywords Rare earths · double perovskite oxides · magnetic cooling · magnetocaloric effect · magnetic properties

Introduction

Solid-state magnetic cooling based on the magnetocaloric (MC) effect^{1–3} of magnetic solids is considered one of the most promising cooling methods^{1–8} due to its remarkable benefits in both social and economic aspects. It is known that the MC effect is a magneto-thermodynamic property^{1–3} which can be identified by the changes in temperature (adiabatic process) or magnetic entropy (isothermal process) with the change in external magnetic field. A crucial prerequisite for this cooling method is the development of magnetic solids with good MC performance. Therefore, many magnetic solids have been fabricated and evaluated systematically in recent decades to assess their MC properties^{9–15} not only for exploring suitable materials for magnetic cooling applications but also for deepening our understanding of their magnetic properties. However, large gaps still exist between the requirements of magnetic cooling applications and the

performance of reported magnetocaloric materials. Thus, the development of suitable candidate materials with large MC effects and promising MC performance remains an urgent research task for magnetic cooling applications.

In recent years, many rare earth (RE)-transition metal (TM)-based magnetic solids^{16–27} have been fabricated and their MC effects determined. Some are reported to exhibit good MC performance and are of great interest for low-temperature magnetic cooling. For example, pure and doped $(\text{RE}_{1-x}\text{A}_x)\text{MnO}_3$ oxides^{16,17} with perovskite-type structure have recently been reported to exhibit good room-temperature MC performance. $\text{RE}(\text{Al}, \text{Co}, \text{Ni})_2$ -based compounds^{19,20} have recently been reported to be good candidate materials for low-temperature magnetic cooling. The magnetic phase transition (MPT) of $\text{RECo}_{12}\text{B}_6$ compounds²¹ were determined by Ma et al. in which considerable reversible MC effects were reported and the MPT obeys the 3D Heisenberg model. The structural and magnetic properties of RE_3RuO_7 oxides²⁴ were determined by He et al., in which large MC effects were reported in Gd_3RuO_7 and Tb_3RuO_7 oxides.²⁴ The MPT and MC properties in RECu_2Si_2 ²⁵ and RECu_2Ge_2 ²⁶ compounds were determined by Wang et al., in which considerable low-temperature reversible MC effects were reported which are related to first-order type MPT. The structural and magnetic properties in $\text{Sr}_2\text{RETaO}_6$ oxides were determined by Xu et al.,²⁷ who reported large

✉ Yikun Zhang
y kzhang@shu.edu.cn

¹ School of Electronics and Information, Hangzhou Dianzi University, Hangzhou 310018, China

² Key Laboratory of Novel Materials for Sensor of Zhejiang Province, Hangzhou Dianzi University, Hangzhou 310012, China

low-temperature reversible MC effects. These studies indicated that there are some RE-based alloys and oxides with high potential to exhibit large MC effects and good MC performance, and are worthy of further study.

The RE-based double perovskite (DP)-type oxides^{28–37} with the general formula $\text{RE}_2\text{TMTM}'\text{O}_6$ have engendered intense research interest in recent years. The $\text{RE}_2\text{TMTM}'\text{O}_6$ DP oxides are derived from the standard ABO_3 -type perovskite^{28–31} where the A-site is occupied by RE elements and the B-site is occupied by two different TM elements. These DP-type oxides were reported to exhibit interesting optical, electrical, and magnetic properties.^{28–37} Moreover, large low-temperature MC effects and good MC performance^{31–37} were also reported in some heavy RE-based DP-type oxides. For example, our group previously fabricated $\text{RE}_2\text{CuMnO}_6$,³² $\text{RE}_2\text{FeAlO}_6$,³³ and $\text{RE}_2\text{CrMnO}_6$ ³⁴ DP oxides and reported considerable low-temperature reversible MC effects. $\text{RE}_2\text{NiTiO}_6$ DP oxides³⁶ were very recently fabricated by Zhang et al., in which a large low-temperature reversible MC effect was reported in $\text{Gd}_2\text{NiTiO}_6$ DP oxide.³⁶ $\text{RE}_2\text{FeCoO}_6$ DP oxides³⁷ were fabricated by Dong et al., in which large low-temperature reversible MC effects were reported. The MPT and magnetic properties of $\text{RE}_2\text{ZnMnO}_6$ DP oxides were determined by Li et al.,³⁸ in which a large low-temperature reversible MC effect was reported in $\text{Gd}_2\text{ZnMnO}_6$ DP oxide,³⁸ which is attractive for low-temperature magnetic cooling. In continuation of our series investigation on magnetic and MC properties of RE-TM-based magnetic solids^{32–35,39–41} and to deepen our understanding of the magnetic properties of $\text{RE}_2\text{TMTM}'\text{O}_6$ DP oxides, we herein fabricated $\text{Tb}_2\text{FeCrO}_6$ DP oxides and experimentally determined their structural, magnetic, MPT, and MC properties. Large reversible MC effects were observed, making the present $\text{Tb}_2\text{FeCrO}_6$ DP oxides applicable for low-temperature magnetic cooling applications as well.

Experimental Detail

Polycrystalline $\text{Tb}_2\text{FeCrO}_6$ DP oxide was fabricated using a solid-state reaction from the oxides of Tb_4O_7 , Fe_3O_4 , and Cr_2O_3 with purity better than 99.9%. Firstly, the raw oxides were weighed in a stoichiometric ratio and ground thoroughly. The obtained mixed powders were then cold-pressed into pellets and sintered at 1020°C for 10 h in alumina crucibles. Next, the obtained pellets were broken into pieces by hand and re-ground. Finally, the powders were again cold-pressed into small thin pellets and annealed at 1120°C in alumina crucibles for another 38 h to obtain the polycrystalline $\text{Tb}_2\text{FeCrO}_6$ DP oxide. X-ray powder diffraction (XRD, Bruker D8 Advance) patterns of $\text{Tb}_2\text{FeCrO}_6$ oxide at room temperature were collected using monochromatic

$\text{Cu-K}\alpha$ radiation. Rietveld refinement of XRD was performed using FullProf software.⁴² The microstructure and elemental composition of $\text{Tb}_2\text{FeCrO}_6$ DP oxide were determined using field-emission scanning electron microscopy (FE-SEM, SM-7800F) coupled with energy-dispersive x-ray spectroscopy (EDS). The magnetization measurements of $\text{Tb}_2\text{FeCrO}_6$ DP oxide were determined using the magnetic property measurement system (MPMS-3, QD).

Results and Discussion

The crystal structure and phase purity of $\text{Tb}_2\text{FeCrO}_6$ oxide were analyzed using room-temperature XRD technology. The experimental XRD patterns with fitting curves for $\text{Tb}_2\text{FeCrO}_6$ oxide are presented in Fig. 1. All the observable diffraction peaks are consistent with a double perovskite (DP)-type structure belonging to the space group $Pbnm$. The lattice parameters a , b , and c for $\text{Tb}_2\text{FeCrO}_6$ DP oxide are determined to be 5.292, 5.562, and 7.596 Å, respectively. The reliability factors of R_b , R_{wp} , and R_{exp} for $\text{Tb}_2\text{FeCrO}_6$ DP oxide are 4.89%, 6.73%, and 2.84%, respectively. These small values confirm good accordance between the experimental and refined patterns, indicating high purity and single-phase characteristics. The microstructure and phase homogeneity of $\text{Tb}_2\text{FeCrO}_6$ DP oxide were checked using SEM, as presented in Fig. 2. The size and distribution of the grains are almost uniform, indicating good homogeneity. The distribution of constituent elements was further checked using the area EDS mapping analysis. The mapping results for $\text{Tb}_2\text{FeCrO}_6$ DP oxide with constituent elements Tb, Fe, Cr, and O are presented in Fig. 2b–e, respectively. Notably, these elements are uniformly distributed at the micrometer scale, confirming the homogeneity of $\text{Tb}_2\text{FeCrO}_6$ DP oxide.

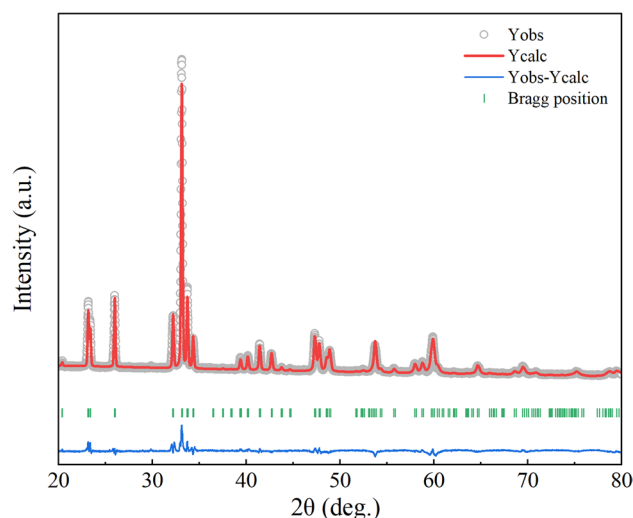


Fig. 1 XRD patterns for $\text{Tb}_2\text{FeCrO}_6$ DP oxide.

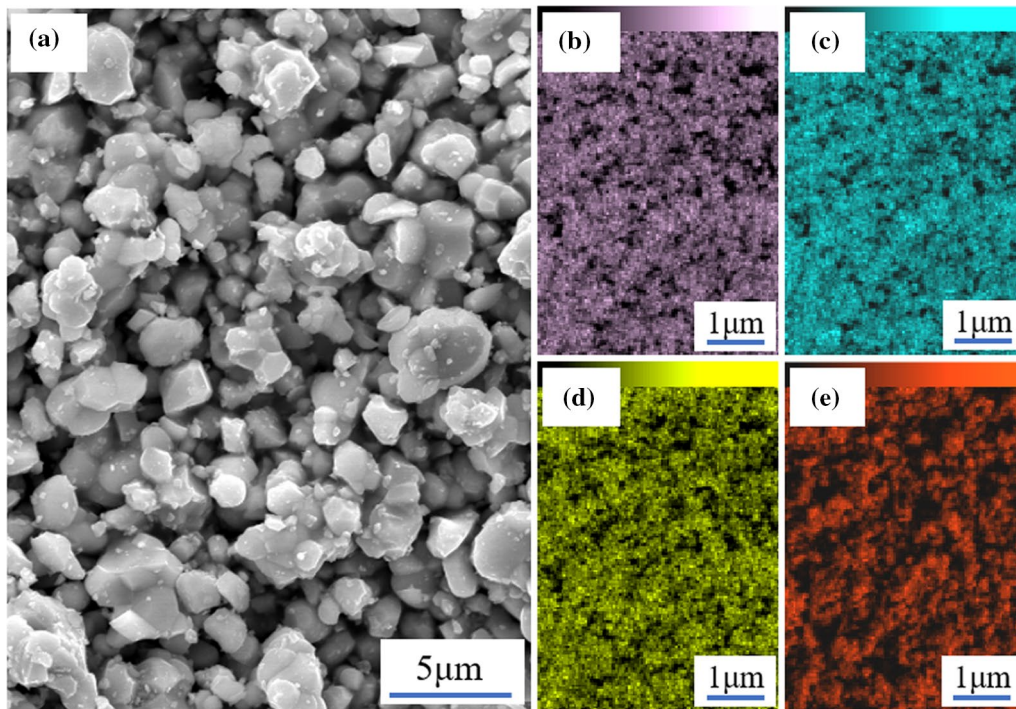


Fig. 2 (a) SEM images for Tb₂FeCrO₆ DP oxide and (b–d) EDS mapping results of Tb, Fe, Cr, O in Tb₂FeCrO₆ DP oxide.

The average atomic ratios were determined to be 19.6 at.% for Tb, 9.2 at.% for Fe, 12.5 at.% for Cr, and 58.7 at.% for O, respectively, which are consistent with the expected chemical composition (2:1:1:6). Thus, the XRD, SEM and EDS results all confirmed that the studied Tb₂FeCrO₆ DP oxide has high purity, good homogeneity, and single-phase characteristics.

Temperature (T)-dependent magnetization (M) was assessed to understand the magnetic transition of Tb₂FeCrO₆ DP oxide. The field-cooling (FC) and zero-field-cooling (ZFC) $M(T)$ curves for Tb₂FeCrO₆ DP oxide are presented in Fig. 3a with a magnetic field (H) of 0.2 T. Significant signals from paramagnetic (PM)-to-antiferromagnetic (AFM) transition for Tb₂FeCrO₆ DP oxide with a magnetic transition temperature (T_N) of around ~ 8.5 K can be noted. Moreover, only a slight difference is found between the FC and ZFC curves at the low-temperature range for Tb₂FeCrO₆ DP oxide, demonstrating weak thermal hysteresis which is good for magnetic cooling applications. The $M(T)$ curve (corresponding to the left scale) together with the inverse susceptibility ($1/\chi = H/M$; corresponding to the right scale) for Tb₂FeCrO₆ DP oxide are presented in Fig. 3b, with H of 1 T. Notably, the $1/\chi(T)$ curves in the PM region for Tb₂FeCrO₆ DP oxide obeying the Curie–Weiss law,

$$\chi(T) = C/(T - \theta_p), \quad (1)$$

where C and θ_p represent the Curie constant and paramagnetic Curie temperature, respectively, and $C = N(\mu_B \mu_{\text{eff}})^2 / 3\kappa_B$ (where μ_{eff} denotes the effective magnetic moment). The linear fittings from 50 K to 150 K produced a negative θ_p value of -2.7 K for Tb₂FeCrO₆ DP oxide, which further confirms the AFM transition. The corresponding value of μ_{eff} was determined to be $10.89 \mu_B/\text{RE}$, which is larger than when only considering the theoretical magnetic moment of Tb³⁺ ions ($9.72 \mu_B$). These results indicate that the Fe and/or Cr ions also play crucial roles in the magnetism of Tb₂FeCrO₆ DP oxide.

To explore the MC performance of Tb₂FeCrO₆ DP oxide, series magnetization isotherms, the $M(H)$ curves, were determined and are presented in Fig. 4a. For the low-temperature curves, the values of M for Tb₂FeCrO₆ DP oxide increased linearly with increasing H in the low H region, showing a saturation-like behavior in the high H region. Moreover, the MC effect and MC performance are strongly related to the corresponding nature of the magnetic transition. According to the Banerjee criterion,⁴³ the magnetic transition is of first-order (FO) type if some of the Arrott plots (H/M versus M^2) show negative slopes, whereas once all the Arrott plots have positive slopes, this transition becomes second-order (SO). Therefore, to examine the order type of the magnetic transition, the Arrott plots (H/M versus M^2) for Tb₂FeCrO₆ DP oxide, as presented in Fig. 4b, were obtained based on the Banerjee law,⁴³ where the results were directly transferred based on

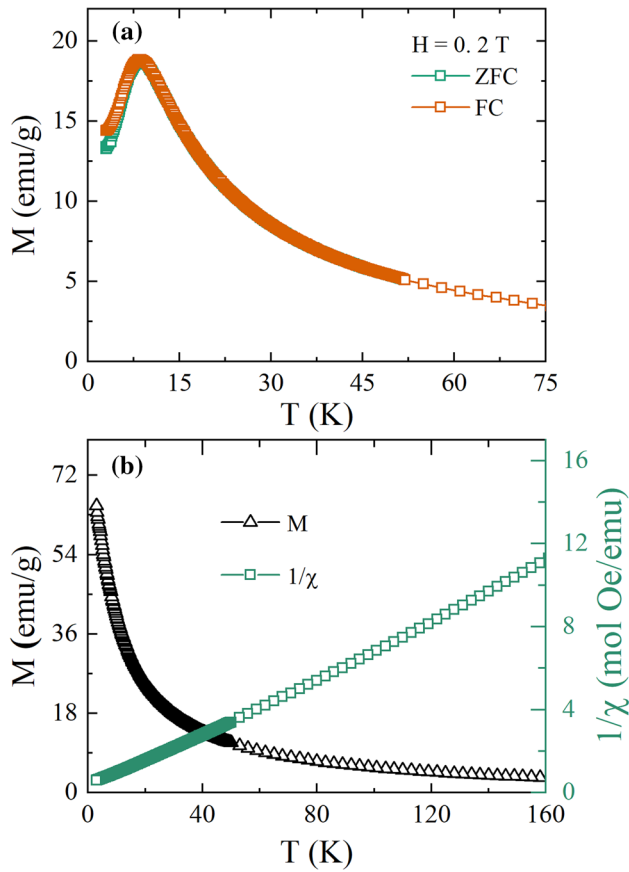


Fig. 3 (a) FC and ZFC $M(T)$ curves with H of 0.2 T for $\text{Tb}_2\text{FeCrO}_6$ DP oxide. (b) $M(T)$ and $1/\chi(T)$ curves with H of 1 T for $\text{Tb}_2\text{FeCrO}_6$ DP oxide.

the above $M(H)$ data. The Arrott plots exhibited negative slopes in $\text{Tb}_2\text{FeCrO}_6$ DP oxide for the low-temperature curves at the low H region, as presented in the inset of Fig. 4b, demonstrating the presence of FO type magnetic transition for $\text{Tb}_2\text{FeCrO}_6$ DP oxide.

The MC effect and MC performance are estimated primarily by the values of magnetic entropy change, ΔS_M , which can be indirectly calculated using the following equations,^{32–35}

$$\Delta S_M(T, \Delta H) = S_M(T, H) - S_M(T, 0) = \int_0^{H_{\max}} \left(\frac{\partial S(H, T)}{\partial H} \right)_T dH, \quad (2)$$

based on the Maxwell thermodynamic relation,

$$\left(\frac{\partial S(H, T)}{\partial H} \right)_T = \left(\frac{\partial M(H, T)}{\partial T} \right)_H; \quad (3)$$

then,

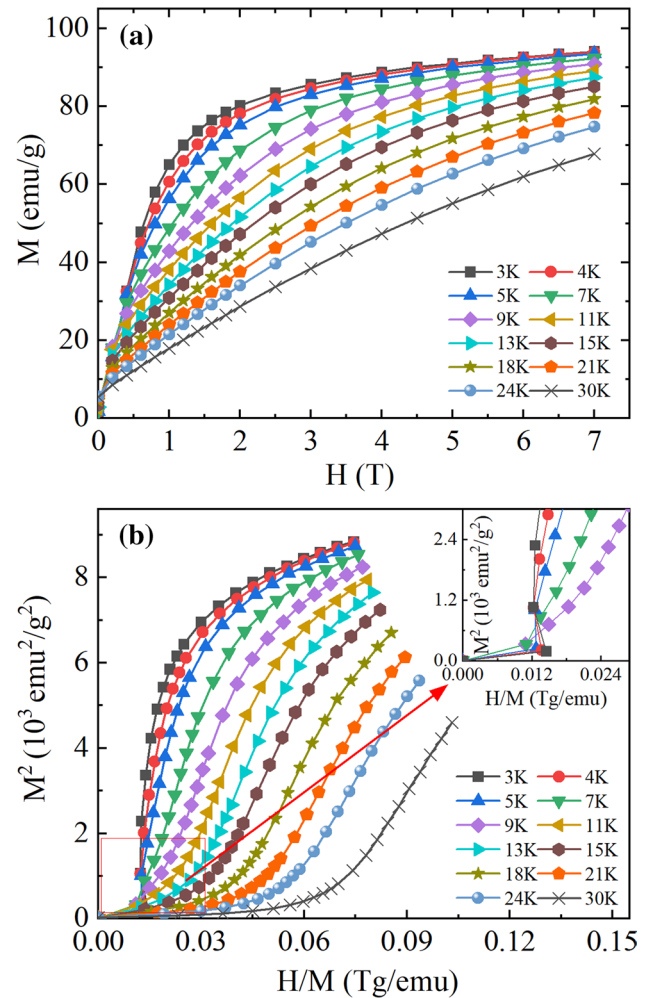


Fig. 4 (a) $M(H)$ curves for $\text{Tb}_2\text{FeCrO}_6$ DP oxide. (b) Arrott plots (H/M versus M^2) for $\text{Tb}_2\text{FeCrO}_6$ DP oxide.

$$\Delta S_M(T, \Delta H) = S_M(T, H) - S_M(T, 0) = \int_0^{H_{\max}} \left(\frac{\partial M(H, T)}{\partial T} \right)_H dH, \quad (4)$$

Thus, the ΔS_M values can be calculated from the experimentally obtained $M(H)$ data by:

$$\Delta S_M(T, \Delta H) \approx \sum_i \frac{M_{i+1}(T_{i+1}, H) - M_i(T_i, H)}{T_{i+1} - T_i} \Delta H. \quad (5)$$

The calculated temperature-dependent $-\Delta S_M$ curves for $\text{Tb}_2\text{FeCrO}_6$ DP oxide are presented in Fig. 5a. The $-\Delta S_M$ values increase gradually with the increases in ΔH . Under ΔH of 0–3, 0–5 T, and 0–7 T, the maximum $-\Delta S_M$ values ($-\Delta S_M^{\max}$) found for $\text{Tb}_2\text{FeCrO}_6$ DP oxide are 7.8, 11.0, 12.9 J/kg K, respectively. Moreover, the $-\Delta S_M^{\max}$ and the respective peak temperatures (T^{peak}) gradually shifted to higher temperatures with increasing ΔH . Additionally, a

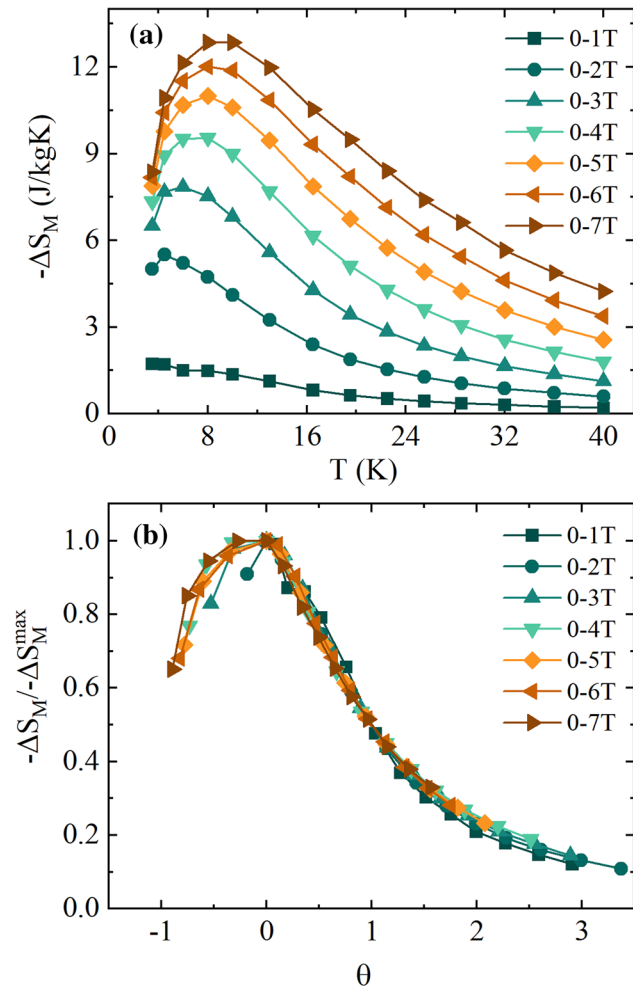


Fig. 5 (a) $-\Delta S_M$ curves for Tb₂FeCrO₆ DP oxide. (b) Constructed $\Delta S_M / \Delta S_M^{\max}$ versus θ curves for Tb₂FeCrO₆ DP oxide.

phenomenological $-\Delta S_M(T)$ universal curve⁴⁴ for the MC materials was proposed by changing the Y and X axes to $\Delta S_T(T) / \Delta S_M^{\max}$ and θ , respectively. The θ is expressed above and below T_C independently, as follows:

$$\theta = \begin{cases} -(T - T_C) / (T_{r1} - T_C) & \text{for } T \leq T_C \\ (T - T_C) / (T_{r2} - T_C) & \text{for } T > T_C \end{cases} \quad (6)$$

Here, T_{r1} and T_{r2} ($T_{r1} < T_C < T_{r2}$), corresponding to $\Delta S(T_{r1}, T_{r2}) = 0.6 \times \Delta S_M^{\max}$, are two reference temperatures. The constructed $\Delta S_M / \Delta S_M^{\max}$ versus θ curves for Tb₂FeCrO₆ DP oxide are presented in Fig. 5b. Obvious deviation can be observed in the low-temperature region, further confirming the presence of a FO-type magnetic transition for Tb₂FeCrO₆ DP oxide.

In addition to $-\Delta S_M$, the parameters of temperature-averaged entropy changes (TEC, as given in Eq. 7)^{32–35,45}

and relative cooling power (RCP, as given in Eq. 8)^{32–35} have also been widely used to assess the performance of MC materials based on experimentally obtained $-\Delta S_M(T)$ results.

$$\text{TEC}(\Delta T_{\text{lift}}) = \frac{1}{\Delta T_{\text{lift}}} \max_{T_{\text{mid}}} \left\{ \int_{T_{\text{mid}} - \frac{\Delta T_{\text{lift}}}{2}}^{T_{\text{mid}} + \frac{\Delta T_{\text{lift}}}{2}} \Delta S_M(T) \Delta H, T \, dT \right\}, \quad (7)$$

$$\text{RCP} = |\Delta S_M^{\max}| \times \delta T_{\text{FWHM}}, \quad (8)$$

where T_{mid} represents the central temperature at which $\text{TEC}(\Delta T_{\text{lift}})$ reaches the maximum value. Here, ΔT_{lift} of 3 and 5 K was selected at around T_N , and the resulting $\text{TEC}(3)/\text{TEC}(5)$ values for Tb₂FeCrO₆ DP oxide under ΔH of 0–3, 0–5, and 0–7 T were found to be 7.7/7.6 J/kg K, 10.9/10.8 J/kg K, and 12.8/12.7 J/kg K, respectively. The corresponding values of RCP were 122.7 J/kg, 230.3 J/kg, and 341.4 J/kg, respectively. Then, the MC performance of Tb₂FeCrO₆ DP oxide was compared with recently reported RE-based oxide candidate materials. The above-mentioned MC parameters of $-\Delta S_M^{\max}$, $\text{TEC}(5)$, and RCP for Tb₂FeCrO₆ DP oxide are lower than those of some of the famous Gd-based magnetocaloric materials,^{35–38} whereas they are at similarly high level as the recently updated low-temperature RE-based MC materials including RE₂CrMnO₆,³⁴ RENiGa₂,⁴⁶ RE₃RuO₇,²⁴ GdFe₂Si₂,⁴⁷ RE₂BaZnO₅,⁴⁸ RECu₂Ge₂,²⁶ Sr₂RETaO₆,²⁷ and RE₂CuMnO₆,³² making Tb₂FeCrO₆ DP oxide a good candidate for low-temperature magnetic cooling applications as well.

Conclusions

In summary, a single-phase polycrystalline Tb₂FeCrO₆ DP oxide was fabricated and its structure, magnetic transition, MC effect, and MC performance were investigated. The Tb₂FeCrO₆ DP oxide is crystallized in a double perovskite-type structure with *Pbnm* space group and undergoes a PM-to-AFM transition at a temperature of ~ 8.5 K. Large MC effects and considerable MC performance were observed. The $-\Delta S_M^{\max}$, $\text{TEC}(5)$, and RCP values obtained for Tb₂FeCrO₆ DP oxide under ΔH of 0–7 T are 12.9 J/kg K, 12.7 J/kg K, and 341.4 J/kg, respectively. These findings indicate that Tb₂FeCrO₆ oxide can be considered a good candidate for magnetic cooling applications at low temperatures.

Conflict of interest The authors declare that they have no conflict of interest.

References

1. T. Gottschall, K.P. Skokov, M. Fries, A. Taubel, I. Radulov, F. Scheibel, D. Benke, S. Riegg, and O. Gutfleisch, Making a cool choice: the materials library of magnetic refrigeration. *Adv. Energy Mater.* 9, 1901322 (2019).
2. J.Y. Law, L.M. Moreno-Ramírez, Á. Díaz-García, and V. Franco, Current perspective in magnetocaloric materials research. *J. Appl. Phys.* 133, 040903 (2023).
3. Y.K. Zhang, W.X. Hao, C.L. Hu, X. Wang, X.F. Zhang, and L.W. Li, Rare-earth-free $\text{Mn}_{30}\text{Fe}_{20-x}\text{Cu}_x\text{Al}_{50}$ magnetocaloric materials with stable cubic CsCl-type structure for room-temperature refrigeration. *Adv. Funct. Mater.* 33, 2310047 (2023).
4. D.Y. Cong, W. Xiong, A. Planes, Y. Ren, L. Mañosa, P. Cao, Z. Nie, X. Sun, Z. Yang, X. Hong, and Y.D. Wang, Colossal elastocaloric effect in ferroelastic Ni-Mn-Ti Alloys. *Phys. Rev. Lett.* 122, 255703 (2019).
5. B. Li, Y. Kawakita, S. Ohira-Kawamura, T. Sugahara, H. Wang, J. Wang, Y. Chen, S.I. Kawaguchi, S. Kawaguchi, K. Ohara, K. Li, D. Yu, R. Mole, T. Hattori, T. Kikuchi, S. Yano, Z. Zhang, Z. Zhang, W. Ren, S. Lin, O. Sakata, K. Nakajima, and Z.D. Zhang, Colossal barocaloric effects in plastic crystals. *Nature* 567, 506 (2019).
6. J.C. Lin, P. Tong, X.K. Zhang, Z.C. Wang, Z. Zhang, B. Li, G.H. Zhong, J. Chen, Y.D. Wu, H.L. Lu, L.H. He, B. Bai, L.S. Lin, W.H. Song, Z.D. Zhang, and Y.P. Sun, Giant room-temperature barocaloric effect at the electronic phase transition in $\text{Ni}_{1-x}\text{Fe}_x\text{S}$. *Mater. Horiz.* 7, 2690 (2020).
7. J. Lin, P. Tong, K. Zhang, W. Lu, X. Wang, X. Zhang, W. Song, and Y. Sun, Colossal and reversible barocaloric effect in liquid-solid-transition materials n-alkanes. *Nat. Commun.* 12, 596 (2022).
8. Z.P. Ma, X.S. Dong, Z.Q. Zhang, and L.W. Li, Achievement of promising cryogenic magnetocaloric performances in $\text{La}_{1-x}\text{Pr}_x\text{Fe}_{12}\text{B}_6$ compounds. *J. Mater. Sci. Technol.* 92, 138–142 (2021).
9. J.Y. Law, and V. Franco, Pushing the limits of magnetocaloric high-entropy alloys. *APL Mater.* 9, 080702 (2021).
10. Q. Shen, I. Batashev, F. Zhang, H. Ojiyed, I. Dugulan, N. van Dijk, and E. Brück, Exploring the negative thermal expansion and magnetocaloric effect in $\text{Fe}_2(\text{Hf}, \text{Ti})$ Laves phase materials. *Acta Mater.* 257, 119149 (2023).
11. Y.K. Zhang, P. Xu, J. Zhu, S.M. Yan, J.C. Zhang, and L.W. Li, The emergence of considerable room temperature magnetocaloric performances in the transition metal high-entropy alloys. *Mater. Today Phys.* 32, 101031 (2023).
12. G. Yao, B. Liu, Q. Wang, W. Cui, and S. Yang, Magnetic transition and magnetocaloric effect of Gd (Ga, X) (X = Al, Si) alloys. *J. Electron. Mater.* 5, 23742 (2023).
13. Z. Guan, J. Bai, Y. Zhang, J. Gu, N. Morley, Y.D. Zhang, C. Esling, X. Zhao, and L. Zuo, Ni-Co-Mn-Ti-B high performance multiferroic phase transformation material: simultaneous modulation of mechanical properties and successive caloric effects by B doping. *Mater. Today Phys.* 36, 101183 (2023).
14. Y.K. Zhang, W.X. Hao, J. Shen, Z. Mo, T. Gottschall, and L.W. Li, Investigation of the structural and magnetic properties in the GdCoC compound featuring excellent cryogenic magnetocaloric performances. *Acta Mater.* (2024), in press.
15. Y. Zhang, B. Wu, D. Guo, J. Wang, and Z. Ren, Magnetic properties and promising cryogenic magneto-caloric performances of $\text{Gd}_{20}\text{Ho}_{20}\text{Tm}_{20}\text{Cu}_{20}\text{Ni}_{20}$ amorphous ribbons. *Chin. Phys. B* 30, 017501 (2021).
16. W. Zhang, Z. Xie, Z. Zou, X. Jiang, C. Xu, and M. Feng, Eu/Ni doping on the structure, magnetocaloric effect and critical behaviour of $\text{La}_{0.65}\text{Sr}_{0.35}\text{MnO}_3$ ceramics. *Ceram. Int.* 50, 4291 (2024).
17. X. Jiang, Z. Zou, B. He, W. Zhang, and Z. Mao, Large magnetocaloric effect of Sm^{3+} -doped $\text{La}_{0.7}\text{Sr}_{0.3-x}\text{Sm}_x\text{Mn}_{0.95}\text{Ni}_{0.05}\text{O}_3$ ($x=0, 0.05, 0.10, 0.15$) manganites near room temperature. *J. Electron. Mater.* 52, 4587 (2023).
18. L.W. Li, and M. Yan, Recent progresses in exploring the rare earth based intermetallic compounds for cryogenic magnetic refrigeration. *J. Alloy. Compd.* 823, 153810 (2020).
19. J.W. Xu, X.Q. Zheng, L. Xi, X. Kan, B. Bao, T. Ma, Y. Zang, D. Wang, Y. Gao, J. Xu, W. Yin, B.G. Shen, and S.G. Wang, Significant enhancement of magnetocaloric effects via tuning Curie temperature and magnetic anisotropy in rare-earth based compounds. *Appl. Mater. Today* 35, 101982 (2023).
20. Y.K. Zhang, J.Y. Ying, X.Q. Gao, Z.J. Mo, J. Shen, and L.W. Li, Exploration of the rare-earth cobalt nickel-based magnetocaloric materials for hydrogen liquefaction. *J. Mater. Sci. Technol.* 159, 163 (2023).
21. Z. Ma, P. Xu, J. Ying, Y. Zhang, and L. Li, Insight into the structural and magnetic properties of $\text{RECo}_{12}\text{B}_6$ (RE = Ce, Pr, Nd) compounds: a combined experimental and theoretical investigation. *Acta Mater.* 247, 118757 (2023).
22. X. Wang, L.F. Wang, N.L. Gulay, L.W. Li, and R. Pottgen, Magnetic phase transition and magnetocaloric effect of RE_2RuIn (RE = Dy, Ho, Er, Tm). *J. Magn. Magn. Mater.* 589, 171406 (2024).
23. Y.K. Zhang, N.Z. He, Z.Q. Zhang, and X. Wang, Structural, magnetic and magnetocaloric properties of the rare earth (RE) molybdate RE_2MoO_6 (RE = Dy, Tb and Gd) oxides. *Ceram. Int.* 483, 1672 (2022).
24. N. He, P. Wang, J. Huang, X. Wang, Y. Zhang, L. Hu, L. Li, and M. Yan, Structural, magnetic and magnetocaloric properties in the rare earth ruthenate RE_3RuO_7 (RE = Pr, Nd, Gd and Tb) oxides with fluorite related structure. *Ceram. Int.* 48, 36968 (2022).
25. X. Wang, Y. Ma, and Z. Zhang, Magnetic properties and magnetocaloric effect (MCE) in the rare-earths (RE) based RECu_2Si_2 (RE = Nd and Pr) compounds. *Solid State Commun.* 345, 114696 (2022).
26. X. Wang, Y. Ma, and Z. Zhang, Structural and cryogenic magnetic properties of the ternary RECu_2Ge_2 (RE = Pr and Nd) compounds. *J. Electron. Mater.* 51, 5664 (2022).
27. P. Xu, X. Jin, R. Xing, J. Zhao, and L. Li, Magnetic and magnetocaloric properties in $\text{Sr}_2\text{RETaO}_6$ (RE = Dy, Ho, and Er) compounds. *J. Electro. Mater.* 51, 6525 (2022).
28. A. Hossain, P. Bandyopadhyay, and S. Roy, An overview of double perovskites $\text{A}_2\text{B}'\text{B}''\text{O}_6$ with small ions at A site: synthesis, structure and magnetic properties. *J. Alloy. Compd.* 740, 414 (2018).
29. W.J. Yin, B.C. Weng, J. Ge, Q.D. Sun, Z.Z. Li, and Y.F. Yan, Oxide perovskites, double perovskites and derivatives for electrocatalysis, photocatalysis, and photovoltaics. *Energy Environ. Sci.* 12, 442 (2019).
30. P. Xu, Z.P. Ma, P. Wang, H. Wang, and L.W. Li, Excellent cryogenic magnetocaloric performances in ferromagnetic $\text{Sr}_2\text{GdNbO}_6$ double perovskite compound. *Mater. Today Phys.* 20, 100470 (2021).
31. L.W. Li, and M. Yan, Recent progress in the development of $\text{RE}_2\text{TMTM}'\text{O}_6$ double perovskite oxides for cryogenic magnetic refrigeration. *J. Mater. Sci. Technol.* 136, 1–12 (2023).
32. Y.K. Zhang, B. Zhang, S. Li, J. Zhu, B. Wu, J. Wang, and Z. Ren, Cryogenic magnetic properties and magnetocaloric effects (MCE) in B-site disordered $\text{RE}_2\text{CuMnO}_6$ (RE = Gd, Dy, Ho and Er) double perovskites (DP) compounds. *Ceram. Int.* 47, 18205 (2021).
33. B.B. Wu, Y.K. Zhang, D. Guo, J. Wang, and Z. Ren, Structure, magnetic properties and cryogenic magneto-caloric effect (MCE) in $\text{RE}_2\text{FeAlO}_6$ (RE = Gd, Dy, Ho) oxides. *Ceram. Int.* 46, 6290 (2021).
34. B. Wu, D. Guo, Y. Wang, and Y. Zhang, Crystal structure, magnetic properties, and magnetocaloric effect in B-site disordered

- RE_2CrMnO_6 ($RE = Ho$ and Er) perovskites. *Ceram. Int.* 46, 11988–11993 (2020).
35. Y.K. Zhang, Y. Tian, Z. Zhang, Y. Jia, S. Li, B. Zhang, J. Wang, and Z. Ren, Magnetic properties and giant cryogenic magnetocaloric effect in B-site ordered antiferromagnetic Gd₂MgTiO₆ double perovskite oxide. *Acta Mater.* 226, 117669 (2022).
 36. Z. Zhang, P. Xu, Y. Jia, and L. Li, Structural, magnetic and magnetocaloric properties in distorted RE₂NiTiO₆ double perovskite compounds. *J. Phys. Energy* 5, 014017 (2023).
 37. Z.Q. Dong, and S. Yin, Structural, magnetic and magnetocaloric properties in perovskite RE₂FeCoO₆ ($RE = Er$ and Gd) compounds. *Ceram. Int.* 46, 1099–1103 (2020).
 38. L. Li, P. Xu, S. Ye, Y. Li, G. Liu, D. Huo, and M. Yan, Magnetic properties and excellent cryogenic magnetocaloric performances in B-site ordered RE₂ZnMnO₆ ($RE = Gd, Dy$ and Ho) perovskites. *Acta Mater.* 194, 354–365 (2020).
 39. Y.K. Zhang, J. Zhu, S. Li, Z.Q. Zhang, J. Wang, and Z.M. Ren, Magnetic properties and promising cryogenic magnetocaloric performances in the antiferromagnetic GdFe₂Si₂ compound. *Sci. China Mater.* 65, 1345–1352 (2022).
 40. Y. Zhang, J. Zhu, S. Li, J. Wang, and Z.M. Ren, Achievement of giant cryogenic refrigerant capacity in quinary rare-earths based high-entropy amorphous alloy. *J. Mater. Sci. Technol.* 102, 66–71 (2022).
 41. Y.K. Zhang, S. Li, L. Hu, X.H. Wang, L. Li, and M. Yan, Excellent magnetocaloric performance in the carbide compounds RE₂Cr₂C₃ ($RE = Er, Ho$, and Dy) and their composites. *Mater. Today Phys.* 27, 100786 (2022).
 42. J. Rodriguez-Carvajal, FULLPROF: a Rietveld and pattern matching analysis program. *Laboratoire Leon Brillouin CEA-CNRS, France* (2007).
 43. B.K. Banerjee, On a generalised approach to first and second order magnetic transitions. *Phys. Lett.* 12, 16–17 (1964).
 44. V. Franco, and A. Conde, Scaling laws for the magnetocaloric effect in second order phase transitions: from physics to applications for the characterization of materials. *Int. J. Refrig.* 33, 465 (2010).
 45. L.D. Griffith, Y. Mudryk, J. Slaughter, and V.K. Pecharsky, Material-based figure of merit for caloric materials. *J. Appl. Phys.* 123, 034902 (2018).
 46. D. Guo, L.M.M. Ramírez, J.Y. Law, Y.K. Zhang, and V. Franco, Excellent cryogenic magnetocaloric properties in heavy rare-earth based HRENiGa₂ ($HRE = Dy, Ho$ or Er) compounds. *Sci. China Mater.* 66, 249 (2023).
 47. X. Wang, Z. Ma, Z. Zhang, and Y. Zhang, Magnetic properties and cryogenic magneto-caloric effect in the antiferromagnetic REFe₂Si₂ ($RE = Dy$ and Tb) compounds. *Appl. Phys. A* 128, 898 (2022).
 48. P. Xu, L. Hu, Z. Zhang, H. Wang, and L.W. Li, Electronic structure, magnetic properties and magnetocaloric performance in rare earths (RE) based RE₂BaZnO₅ ($RE = Gd, Dy, Ho$, and Er) compounds. *Acta Mater.* 236, 118114 (2022).

Publisher's Note Springer Nature remains neutral with regard to jurisdictional claims in published maps and institutional affiliations.

Springer Nature or its licensor (e.g. a society or other partner) holds exclusive rights to this article under a publishing agreement with the author(s) or other rightsholder(s); author self-archiving of the accepted manuscript version of this article is solely governed by the terms of such publishing agreement and applicable law.